Retrieval of optical and physical properties of African dust from multi-wavelength Raman lidar measurements during the "SHADOW" campaign in Senegal

I. Veselovskii[1,2], P. Goloub[3], T. Podvin[3], V. Bovchaliuk[3], Y. Derimian[3], P. Augustin[4], M. Fourmentin[4], D.Tanre[3], M. Korenskiy[1], D.N. Whiteman[5], A. Diallo[6], T. Ndiaye[6], A. Kolgotin[1], O. Dubovik[3]

[1]*Physics Instrumentation Center of GPI, Troitsk, Moscow, 142190, Russia*

[2]*Joint Center for Earth Systems Technology, UMBC, Baltimore, MD, USA*

[3]*Laboratoire d'Optique Atmosphérie, Université de Lille-CNRS, 59650, Villeneuve d'Ascq, France*

[4]*Laboratoire de Physico-chimie de l'atmosphère, Université du littoral côte d'Opale, France*

[5]*NASA GSFC, Greenbelt, MD 20771, USA*

[6]*Institut de Recherche pour le Développement, Dakar, Sénégal*

ABSTRACT

West Africa and the adjacent oceanic regions are very important locations for studying dust properties and their influence on weather and climate. The SHADOW (Study of SaHAran Dust Over West Africa) campaign is performing a multi-scale and multi-laboratory study of aerosol properties and dynamics using a set of in situ and remote sensing instruments at an observation site located at IRD (Institute for Research and Development) Center, Mbour, Senegal (14^0N, 17^0W). In this paper, we present the results of lidar measurements performed during the first phase of SHADOW which occurred in March-April, 2015. The multiwavelength Mie-Raman lidar acquired $3\beta+2\alpha+1\delta$ measurements during this period. This set of measurements has permitted particle intensive properties such as extinction and backscattering Ångström exponents (BAE) for 355/532 nm wavelengths corresponding lidar ratios and depolarization ratio at 532 nm to be determined. The mean values of dust lidar ratios during the observation period were about 53 sr at both 532 nm and 355 nm, which agrees with the values observed during the SAMUM 1 and SAMUM 2 campaigns held in Morocco and Cape Verde in 2006, 2008. The mean value of particle depolarization ratio at 532 nm was 30±4.5%, however during strong dust episodes this ratio increased to 35±5%, which is also in agreement with the results of the SAMUM campaigns. The backscattering Ångström exponent during the dust episodes decreased to ~-0.7, while the extinction Ångström exponent though being negative, was greater than -0.2. Low values of BAE can likely be explained by an increase in the imaginary part of the dust refractive index at 355 nm compared to 532 nm. The dust extinction and backscattering coefficients at multiple wavelengths were inverted to the particle microphysics using the regularization algorithm and the model of randomly oriented spheroids. The analysis performed has demonstrated that the spectral dependence of the imaginary part of the dust refractive index may significantly influence the inversion results and should be taken into account.

1. INTRODUCTION

The impact of desert dust emitted into atmosphere on the Earth's radiation budget is the subject of intense research (Sokolik and Toon, 1996; Balkanski et al., 2007; Mahowald et al., 2010; Formenti et al., 2011, 2014). Due to the wind patterns involved, dust can be transported far away from the main source regions in Africa and Asia allowing dust to be distributed in varying amounts all over the globe. North Africa is the largest source of dust in the world and several field campaigns have been conducted to evaluate dust particle microphysical properties over Western Africa and to study long range transport of Saharan dust (Reid et al., 2003; Tanre et al., 2003; Redelsperger et al., 2006; Haywood et al., 2008; McConnell et al., 2008). During these campaigns, dust particles were studied via aircraft, ground sampling and using sun photometer measurements. However, vertical distribution of dust has received little attention even though dust vertical structure is critical for an improved understanding of dust advection, transport and dust-cloud interactions. The commonly used instrument to evaluate the height profile of dust particle properties is the aerosol lidar. The numerous measurements performed in Europe, America and Asia with multiwavelength Raman and HSRL lidar systems have resulted in a significant amount of information about the vertical distribution of dust intensive properties, such as depolarization, lidar ratios, extinction and backscattering Ångström exponents (Sakai et al., 2003; De Tomasi et al., 2003; Shimizu et al., 2004; Mona et al., 2006; Papayannis et al., 2008; Xie et al., 2008; Ansmann et al., 2012; Burton et al., 2014; Nisantzi et al., 2015). However these measurements were mostly performed at a significant distance from the source area, so the dust particles were aged due to mixing with local aerosols and coating with soluble aerosol species (Li et al., 2009) and may not have well represented the characteristics of the dust upon initial emission.

To analyze the properties of pure dust measurements near the source regions are needed. Such measurements of Saharan dust were performed during the SAMUM1 and SAMUM2 experiments using the assembly of Raman and HSRL lidars (Ansmann et al., 2011). During those measurements the dust episodes and more complicated events, when the dust and smoke layers occurred simultaneously, were studied (Tesche et al., 2009a,b; 2011; Esselborn et al., 2009). However, for the estimation of aerosol radiative forcing not only the particle intensive parameters, but also their microphysical properties, such as size, concentration and the complex refractive index (CRI) are needed. An estimation of the vertical distribution of particle microphysics can be achieved, for example, by combining lidar and sun photometer measurements; a review of such studies can be found in a recent publication (Binietoglou et al., 2015). However in these retrievals the mean radii and refractive indices of particles in the fine and the coarse mode are assumed to be height independent, and only particle volume in each of the modes is permitted to vary. Such assumptions may become invalid when aerosol layers of different origins occur.

The alternative approach to evaluating the vertical distribution of dust properties is to estimate the particle properties from lidar measurements only. Raman (or HSRL) multiwavelength lidars based on a tripled Nd:YAG laser are able to provide three particle backscattering and two extinction coefficients (so called $3\beta+2\alpha$ dataset). Different techniques have been considered to invert these measurements into particle microphysics (Ansmann and Müller, 2005), but the main issue is small number of input measurements (typically five), compared to the numerous parameters needed for describing the aerosol microphysical properties. This implies that the inverse problem is underdetermined and that numerous solutions may reproduce the input measurements with similar accuracy. This family of solutions can be localized by applying constraints to the "search space", i.e. limiting the range of particle radii and refractive indices considered. The additional assumption usually made is that the refractive index is spectrally independent and identical over the whole size range (Müller et al., 1999; Veselovskii et al., 2002). Such an approach has proved to be efficient for aerosol particle size distributions (PSD) with a predominant fine mode as, for example, in the case of biomass burning aerosols (Müller et al., 2005; Veselovskii et al., 2015). However, in the case of dust the inversion of lidar measurements becomes more challenging since the dust PSD contains a strong coarse mode with particle radii extending up to ~ 15 µm and the estimation of properties for such big particles is less accurate when measurements are only performed in the wavelength range of 355-1064 nm. Moreover, dust particles are of irregular shape and Mie theory is thus not applicable for computations of their scattering properties. Also, the imaginary part of the refractive index (RI) of dust is spectrally dependent, with a strong enhancement of the absorption in the UV region (Patterson et al., 1977). And finally, particles in the fine and coarse mode may have different origin, so the size dependence of the refractive index should also be considered. The complexity of the problem outlined above demands the use of assumptions and simplifications in the retrieval algorithms.

A widely used model for treating irregularly shaped particles is the one used in the operational AERONET algorithm that mimics dust scattering properties with an assembly of randomly oriented spheroids (Mishchenko et al., 1997; Dubovik et al., 2006). For typical dust PSDs the AERONET model provides lidar and depolarization ratios which agrees reasonably well with observed values (Wiegner et al., 2009). The first attempts to invert lidar dust measurements into particle microphysics using the spheroids model were recently made (Veselovskii et al., 2010; Di Girolamo et al., 2012; Papayannis et al., 2012) but were applied to lofted layers of aged dust over Europe. The only test of the spheroidal model relevant to pure dust was performed by using the data acquired during the SAMUM-1 and SAMUM-2 campaigns (Müller et al., 2013). Results indicate that the effective radii derived from lidar measurements are in reasonable agreement with the values provided by AERONET and airplane sampling, while differences are significant for the refractive index.

The application of spheroids to the analysis of lidar dust observations is an important step forward when compared to the spherical particle approximation of Mie theory. Still we should keep in mind that spheroid model was not specifically designed for lidar applications where scattering in the backward direction is considered. For instance, as previously discussed (Gasteiger et al., 2011; Müller et al., 2013) the spheroidal model has difficulty in reproducing depolarization ratios (δ) greater than 30%, , values that are representative for pure dust. When using the spheroidal model, such high depolarization ratios can only be obtained when the real (m_R) and imaginary (m_i) parts of the refractive index are less than 1.5 and 0.005, respectively (Dubovik et al., 2006), even though coincident in situ measurements of dust report higher values (Kandler et al., 2011). To investigate these issues, more measurements near the dust origin source and more tests of suitable inversion schemes are needed.

West Africa and the adjacent oceanic regions are very important locations for studying dust properties and their influence on weather and climate. The SHADOW (Study of SaHAran Dust Over West Africa) campaign is performing a multi-scale and multi-laboratory study of aerosol properties and dynamics using a set of in situ and remote sensing instrumentation (multi-wavelength Raman LIDAR, Wind-LIDAR,, nephelometer, aethalometer, sun/lunar photometer, airborne sunphotometer, optical particle counter) in the framework of the CaPPA (Chemical and Physical Processed in The Atmosphere) project (http://www.labex-cappa.fr/). The site is located at IRD (Institue for Research and Development) Center, Mbour, Senegal (14^{0}N, 17^{0}W). The objective of the experiment is to report the optical, chemical and physical properties of the aerosols as well as the source apportionment in a location where aerosol loading can be very large and aerosol type depends on the season. Two enhanced observing periods of 7 weeks are considered: March-April 2015 when dust due to the Harmattan, which is a dry trade wind that transports dust laden air from the Sahara to West Africa (Schwanghart and Schütt, 2008) is dominant, and December 2015-January 2016 when dust and carbonaceous aerosols resulting from fire activities are in variable proportion and transported at different altitudes. Other types of aerosols can also be present such as sulfates from nearby urban areas or maritime aerosols depending on the air mass flow. The mixed state of these various chemical components results in different radiative properties of the aerosols.

We hereinafter focus our study on multiwavelength Mie-Raman lidar measurements performed during the first phase of the SHADOW campaign for the period 8 March - 24 April 2015. During this period approximately 40 day- and night-time measurement sessions were performed and numerous strong dust episodes were observed. Those lidar observations are used for the analysis of the vertical distribution of the dust intensive and microphysical properties. In section 2 we describe the lidar equipment and in section 3 we provide examples of joint measurements of wind and Raman lidars. Section 4 presents day-to-day variation of dust properties and examples of vertical distribution of dust intensive parameters. The results of inversion of lidar measurements into particle microphysics are given in section 5.

2. LIDAR EXPERIMENTAL SET

Data from three lidar systems were available during SHADOW campaign. These systems are: Doppler wind lidar and multiwavelength Mie-Raman lidar.

Doppler lidar

The wind field within the lower troposphere (<5 km) was measured by an eye safe scanning wind lidar (Windcube WLS 100) manufactured by the LEOSPHERE company (www.leosphere.com). This pulsed Doppler lidar operates at 1543 nm with a repetition rate of 10 kHz and uses a heterodyne technique to measure the Doppler shift of laser radiation backscattered by aerosols. Simultaneous measurements of radial wind speed and aerosol backscatter provides information on both aerosol layer stratification and the dynamics of the lower troposphere (Thobois and Soderholm, 2015). More technical details are given by (Kumer et al., 2014; Ruchith and Ernest Raj, 2015).

During this experiment, continuous monitoring of the wind field in the range from 100 m to 5 km with 50 m range resolution was performed. The total scanning cycle included two 180° scans in the vertical plane along East/West and South/North axes with 1° resolution, 360° azimuthal scan with 2° resolution at 5° elevation angle, and line of sight (LOS) profiles at 75° elevation in the four cardinal directions. The duration of the total cycle was approximately 10 minutes. The combination of LOS sequences is used in order to determine the three components of the wind vector vertical profile relying on the Doppler Beam Swinging (DBS) technique (Browning and Wexler, 1968).

Multiwavelength Mie-Raman lidar

The LILAS multiwavelength Mie-Raman lidar is based on a tripled Nd:YAG Spectra Physics INDI laser with a 20 Hz repetition rate, and pulse energy of 90/100/100 mJ at 355/532/1064 nm. The backscattered light is collected by a 40-cm aperture Newtonian telescope, which is inclined at an angle of 47 degrees to the horizon. Measurements were performed from inside the IRD building through a window and 47 deg to horizon was the maximal angle possible.

. The outputs of the detectors (R1924, R9880 PMTs for 355 nm-532 nm spectral range and APD for 1064 nm) are recorded at 7.5 m range resolution using Licel transient recorders that incorporate both analog and photon-counting electronics. The full geometrical overlap of the laser beam and the telescope FOV is achieved at 800 m -1400 m range depending on FOV used. The system is designed for simultaneous detection of elastic and Raman backscatter signals and thus provides three particle backscattering and two extinction coefficients along with depolarization ratio at 532 nm (so called 3β+2α+1δ set). For the calibration of depolarization measurements, the so called ±45° method, (Freudenthaler et al., 2009) was used. The relative uncertainty of depolarization measurements due to calibration is estimated as ±15%. Acquiring Raman backscatter at 408 nm permits profiling the water vapor mixing ratio (WVMR) (Whiteman et al., 1992). For calibration of the WVMR, radiosonde launches from the Dakar airport, located ~70 km from Mbour, were used. The large separation between the lidar and radiosonde locations prevented an accurate calibration of the WVMR so the WVMR data were used mainly to monitor the relative change of the water vapor content. To improve the system capability for particle extinction measurements at 532 nm, rotational Raman (RR) scattering was used instead of vibrational nitrogen Raman scattering at 608 nm (Veselovskii et al., 2015). For each profile, 4000 laser pulses were accumulated so the temporal resolution of the measurements was approximately 3 minutes. The backscattering coefficients and depolarization ratio were calculated with range resolution 7.5 m (corresponding height resolution 5.5.m). Resolution of extinction measurements varied with height from 50 m (at 1000 m) to 125 m at (at 7000 m).

3. TROPOSPHERE STRATIFIACATION AND DYNAMICS

The aerosol layer stratification over the observation site was mixed-up and difficult to analyze. To demonstrate the advantage of the joint use of wind and Raman lidar measurements, we provide an example of observations performed on the night of 15-16 April. The transport paths of different stratified air masses have been studied by using back trajectories from the NOAA HYSPLIT model (http://ready.arl.noaa.gov/HYSPLIT.php).

For period from 23:00 UTC to 7:00 UTC on 15-16 April 2015 night, the time-height sections of the logarithmic range corrected signal (LRCS) is shown in fig.1 while fig.2 shows the horizontal wind speed (color scale) and direction (arrow) deduced from wind lidar and the sonic anemometer wind measurements near the ground. Back trajectories of the air masses ending in Mbour on 16 April 2015 at 2500 m (02:00 UTC, 06:00 UTC), at 900 m (00:00 UTC) and at 700 m (06:00 UTC) are reported in Fig.3. These figures reveal complex stratification and dynamics of the lower troposphere on 15-16 April: we can distinguish four layers (A-D) from 100 m to a height of approximately 3000 m. In parallel, the wind field highlights the appearance of multi-layered wind structure mainly consisted of a northerly wind (downward arrow) prevailing near ground, which changes to an easterly wind (leftward arrow) with height (fig. 2).

- Layer A, located between 1000 m to 3000 m (at 00:00 UTC), is associated with a small northerly wind speed (< 5 m/s) in the lower part of the layer, and a slightly larger easterly wind speed (> 5 m/s) above 2000 m. Layer A can be considered to be a continentalized maritime trade (CMT) wind which is one of oceanic origin that has been progressively altered by continental trade (CT), as follows from the back trajectories shown in fig.3. Therefore, this layer is characterized by a mixture of maritime and continental air.
- Layer B located between 400 m - 800 m at the beginning of the study period rises progressively up to 700 m - 1000 m by the end of the dataset. This layer is characterized by northeasterly winds and high aerosol loading. According to the back trajectories shown in fig. 3, this air mass was transported from a continental area (Mali) and was mainly advected by a southeasterly continental wind (CW).
- Layer C is a nocturnal low-level jet (LLJ). The jet core height is between 250 and 400 m with a maximum jet speed exceeding 15 m/s. The LLJ was observed throughout the night with a thickness that progressively increased with time perhaps being the causative mechanism for the corresponding increase in height of layer B (fig.1). The LRCS values within layer C decrease progressively up to the end of the observation period, perhaps due to dilution of the aerosol loading.
- Finally, layer D corresponds to the nocturnal boundary layer (NBL) characterized by high LRCS values and by small northerly or northwesterly wind speed (< 5 m/s). The NBL top can be deduced from the LRCS profile discontinuity (Seibert et al., 2000) and is estimated as approximately 200-300 m during the night.

Fig.4 shows the particle extinction at 532nm (4-a), water vapor mixing ratio (4-b), lidar ratio (4-c) and depolarization ratio (4-d) both at 532 nm for the same time-height section as in fig. 1 and 2. The water vapor can be used as a convenient tracer to separate dry continental air masses from oceanic air masses that are characterized by higher vapor content. Due to the geometrical overlap factor, the LILAS minimum height of the measurements shown in fig. 4 is 800 m. Still, layer B (CW) is well observed starting at 03:00 UTC (fig.4a) due to the increase of the layer height. The particle extinction α_{532} in layer A increases after 03:00 UTC while the mixing ratio is decreasing (fig.4b). This may indicate that continental air mass advected by CT has become dominant. The lidar ratio LR_{532} of the particles associated with CT is about 55 sr while for CMT as observed during the first part of the observation period, it is lower (about 45 sr). The depolarization ratio δ_{532} is about 30% in layer A and shows a small enhancement up to 35% for layer B. We should mention also, that for air masses which we consider as "continentalized maritime" the particle depolarization ratio is in excess of 25%, implying a significant amount of dust even in this layer.

4. DUST PARTICLE PROPERTIES DERIVED FROM RAMAN LIDAR OBSERVATIONS

4.1. Day-to- day variation of particle intensive parameters

One of the goals of the SHADOW campaign was to study the dust particle intensive parameters such as extinction and backscattering Ångström exponents together with lidar and depolarization ratios. During March-April 2015 about 40 measurement sessions, including both day and night time periods, were performed. In the analysis presented below only night time measurements are considered, and for every session all lidar signals measured during the night are temporally averaged. Moreover, for an evaluation of day-to-day variations of the particle parameters we use only extinction and backscattering coefficients averaged within 1500 – 2000 m height layer, where a high dust concentration is frequently observed. For such extensive averaging the uncertainties of derived parameters are mainly due to the systematical errors. Thus we estimate the uncertainty of extinction and lidar ratio calculation to be below 10% and 15% respectively for both wavelengths. Uncertainties of extinction and backscattering Ångström exponents derivation are estimated to be below ±0.2.

To give an overview of the variation in aerosol loading, the aerosol optical thickness (AOT) at 440 nm together with the extinction Ångström exponent (EAE) $A^{\alpha}_{380/500}$ measured with Cimel sun photometer is reported in Fig.5 for the 10 March-23 April 2015 period. The AOT was relatively low (mainly below 0.4) for 17-28 March, but increased after 28 March reaching values up to 2.0. The high AOTs are associated with low values of the extinction Ångström exponent indicating numerous dust episodes. Fig.6 shows the particle extinction α_{532} together with extinction (EAE) and backscattering (BAE) Ångström exponents $A^{\alpha}_{355/532}$, $A^{\beta}_{355/532}$ derived from the lidar measurements for the same time period. During 28 March – 15 April several strong dust episodes occurred as indicated by averaged over night particle extinction values as high as 0.5

km^{-1}. The insert in fig.6 provides the frequency distribution of observed EAE and BAE values. EAE varies in -0.15 - 0.3 range, while BAE presents stronger variation, because it is more sensitive to the change of complex refractive index (CRI) and decreases to as low a value as -0.55 during dust events.

The day-to-day variation of the lidar ratios at 355 nm and 532 nm together with particle depolarization ratio at 532 nm is shown in fig.7. The lidar ratios at both wavelengths vary in the 40-65 sr range and the frequency distribution for the ratio LR_{355}/LR_{532} is given by insert in fig.7. In 60% of the cases the ratio LR_{355}/LR_{532} is close to 1, but during dust events this ratio increased up to 1.4. The mean values of lidar ratios are close: LR_{355}=54±8 sr and LR_{532}=53±8 sr. The mean value of particle depolarization ratio is 30±4.5%, however during the dust events depolarization ratio could increase up to 35±5%.

4.2. Vertical distribution of particle intensive properties

The vertical distribution of particle intensive properties is strongly influenced by the origin of the air masses which during the SHADOW measurement period were coming either from ocean or continental regions. In this section, we present the results for three days (13, 29 March and 10 April) characterized by different types of air masses.

13 March

As follows from fig.8, on 13 March at 21:00 UTC the air masses at the 3 heights (1500, 2500 and 3500m) were transported mainly over the ocean, but the back trajectory at 1500 m presents a “loop” over continent, so the corresponding air masses may contain more dust compared to other heights. The relative humidity measured with meteorological sonde in Dakar was below 38% inside 1000 m – 2600 m height range and it increased up to 75% above 3350 m. Fig.9 shows the vertical profiles of 3β+2α measurements together with lidar ratios LR_{355}, LR_{532}, depolarization ratio δ_{532}, and Ångström exponents $A^{\alpha}_{355/532}$, $A^{\beta}_{355/532}$ on 13 March 2015 averaged over the 20:30-21:30 time period. The aerosol layer extended up to 3500 m but the extinction coefficient α was relatively small; at both 355 and 532 nm wavelengths α did not exceed 0.16 km^{-1}. The particle depolarization ratio at 532 nm was approximately 31±4.5% inside the dust layer (up to ~2750 m) and decreased to less than 15% at 3250 m. Likewise, the $A^{\alpha}_{355/532}$ and $A^{\beta}_{355/532}$ are close to zero up to 2750 m, but start to increase above indicating the presence of smaller particles. The lidar ratios LR_{355} and LR_{532} are approximately 53±8 sr inside the dust layer. Above 2750 m the values of LR are more noisy but do not seem to change.

29 March

The backtrajectories from the night of 29-30 March associated to a strong dust case are shown in Fig.10. The air masses at low altitude were transported over the continent and were strongly loaded with dust. The relative humidity was below 19% in 600 m – 1500 m height range Fig.11 presents the vertical profiles of the same particle parameters as in fig.10 but for 29 March. The extinction coefficient α inside the dust layer (below 1500 m) is greater than 0.6 km^{-1} for both wavelengths. The backscattering coefficient β_{355} nm inside the dust layer is lower than β_{532} which is consistent with the lidar ratio R larger at 355 nm than that at 532 nm with values as large as 65 sr. The $A^{\beta}_{355/532}$ (BAE) is negative and gets near -0.8, while EAE is still close to 0 as observed on 13 March (Fig.9). The negative values of BAE can result from the spectral dependence of the imaginary part of the dust refractive index (RI) which is larger at 355 than at 532 nm (e.g. Patterson et al., 1977; Ansmann et al., 2011).

The ground based measurements performed during the SAMUM campaign demonstrated that the imaginary part of the dust RI could vary from m_I=0.005 at 532 nm to m_I=0.02 at 355 nm (Ansmann, et al., 2011). Such a strong enhancement of m_I may lead to a decrease of the backscattering coefficient (Veselovskii et al., 2010). To estimate the impact of the m_I enhancement at 355 nm on the values of EAE and BAE at 355/532 nm wavelengths, numerical simulations were performed. Extinction and backscattering Ångström exponents were calculated using the model of randomly oriented spheroids as described in (Veselovskii et al., 2010) for a bimodal particle size distribution:

$$\frac{dn(r)}{d\ln(r)} = \sum_{i=f,c} \frac{N_i}{(2\pi)^{1/2}\ln\sigma_i} \exp\left[-\frac{(\ln r - \ln r_i)^2}{2(\ln\sigma_i)^2}\right]. \qquad (1)$$

where $N_{f,c}$ is particle number density in the fine (*f*) and the coarse (*c*) mode. Each mode is represented by a lognormal distribution with modal radius $r_{f,c}$ and dispersion $\ln\sigma_{f,c}$. For the fine mode, values of r_f=0.1 µm and $\ln\sigma_f$ =0.4 were used. For the coarse mode r_c=1.0 µm and three values $\ln\sigma_c$ =0.4, 0.5, 0.6 were considered. The three size distributions expressed in volume are reported in the insert of fig.12. The ratio N_c/N_f in all cases was 0.01, and the real part of CRI was 1.55 for all wavelengths. The imaginary part was fixed at 0.005 for 532 nm while it varied within the 0.005 – 0.05 range at 355 nm. Values of EAE and BAE as a function of m_I at 355 nm are given by fig.12. The EAE shows no significant sensitivity to changes in m_I, but BAE decreases rapidly as a function of m_I at 355 nm. The present sensitivity study is limited but illustrates the importance of accounting for the right spectral dependence of $m_I(\lambda)$.

10 April

On April 10, the air masses were coming from continental regions and particle parameters showed large variation with height. We selected measurements during the period 0:00-2:00 UTC for which the backward trajectories at 1:00 UTC are shown in fig.13. The air masses at 2000 m and 3000 m originate from the dust-laden continental region (Barren or sparsely vegetated areas), while at 4500 m the air masses come from regions covered by grass lands and savannas. Fig.14 shows profiles of the 3β+2α measurements together with particle intensive parameters. The particle extinction increases with height reaching a maximum value of around 0.2 km^{-1} for both wavelengths at a height of approximately 3000 m and then decreases up to 5 000m. The EAE is approximately zero up to 3000 m and then it increases to 1.0 at 4500 m. The BAE below 3000 m is smaller with minimum value $A^{\beta}_{355/532}$ ≈-0.5, but increase up to 4500 m where EAE and BAE are approximately equivalent. The depolarization ratio is around 30% in the 2000-3500 m range, and decreases for higher altitudes. The lidar ratio at 355 nm inside 2000-3500 m layer exceeds that at 532 nm (averaged values are 60±9 sr and 53±8 sr correspondingly) and for higher altitudes the lidar ratios at both wavelengths are close. So we can identify different aerosol layers with different properties: mostly pure dust layer within the 2000-3500 m altitude range and mixed aerosols above it.

The relative humidity on 10 April was higher than on 13, 29 March, which could impact the particle properties. Fig.15 shows the estimated profile of water vapor mixing ratio (WVMR) obtained from the lidar measurements. WVMR is less than 3 g/kg within the dust layer and increases above 3500 m reaching approximately 5.5 g/kg at 4000 m. The WVMR and the relative humidity measured in Dakar at 0:00h using a radiosounding is reported on Fig.15 for comparison. Both WVMR's measured by sounding and lidar are in agreement between 3000m and 5000m (note that there is no sounding data between 4620 m and 3880 m). There are clearly two distinct layers. If the derived properties of aerosols within the lower layer are representative of dust, the air mass above 4000m brings another particle type. Particles, characterized by lower depolarization ratio, are smaller since the EAE is increasing, and the layer is more humid since the RH is increasing. Based on the analysis of the satellite data quick-looks (see for instance http://earthobservatory.nasa.gov/GlobalMaps/), the back-trajectories reporting in Fig. 13 show that the air mass at 4500m is coming from regions where fires were active during several days, which can result in emission of smoke particles transported over M’Bour few days later. The derived properties of aerosols within the 4000-5000m layer are consistent with this hypothesis; the assumption of the air-mass origin is also consistent with the RH increase.

5. INVERSION OF RAMAN LIDAR OBSERVATIONS TO THE PARTICLE MICROPHYSICS

The lidar $3\beta+2\alpha$ and $3\beta+2\alpha+1\delta$ observations analyzed in the previous sections can be inverted into microphysical properties using regularization algorithm. As previously mentioned, in the case of irregularly shaped dust particles such inversion is more complicated compared to other aerosol types that may be well handled by spherical particle assumptions. In an earlier study, a model of randomly oriented spheroids for dust was used (Veselovskii et al., 2010). This model handles the dust particles as a mixture of spheres and spheroids, so an additional unknown parameter, spheroids volume fraction (SVF), appears. The SVF in principle can be determined in the process of inversion of $3\beta+2\alpha+1\delta$ measurements thanks to the use of depolarization ratio as input parameter. However, for the dust layers, in a first guess, we assume a value of SVF=100% to decrease the number of retrieved parameters. In the process of inversion we used algorithm from (Veselovskii et al., 2010) and the “search space” parameters similar to those described in (Müller et al., 2013). The boundary of the inversion window has been set to minimum and maximum particle radii of 0.075 and 15 μm, respectively. The real part of RI was allowed to vary in the range 1.35 - 1.65, while the imaginary part varied in the range 0 - 0.02. The refractive index was assumed to be spectrally independent. The effects of a possible spectral dependence of the imaginary part of RI will be considered at the end of this section.

Fig. 16 shows the particle volume density retrieved from $3\beta+2\alpha$ measurements on 13 March, 29 March and 10 April, which were discussed in the 4.2 section. The profiles of particle volume are given together with corresponding extinction coefficients at 532 nm. The volume – extinction ratio V/α_{532} for these days is also reported as an insert. Inside the dust layer this ratio varies within the range (0.50-0.65)*10^{-6} m, while outside the dust layer, the V/ α_{532} ratio decreases. An overview of observed values of the volume – extinction ratio for dust, obtained from in situ, AERONET and lidar measurements is presented in Ansmann et al., 2012 and provides V/ α_{532} varying within the range (0.60-1.29)*10^{-6} m. Thus our results are near the low boundary of these previously published results.

The profiles of the effective radius and the real part of RI are shown in fig.17. The inverted effective radius inside the dust layer is between 1.05 and 1.25µm (1.15±0.3 µm) and similar for the 3 days. The AERONET retrievals provided column integrated values that are in the same range and agrees within the uncertainty. On 30 March early morning, when the dust contribution to the AOT is prevailing, the effective radius r_{eff}=1.36 µm and it varies between 0.918 and 1.70 depending on the days and time. The lidar retrievals indicate that the real part of the CRI in the dust layer varied from 1.51±0.05 to 1.57±0.05, which is quite typical for desert dust (Patterson et al., 1977), while the AERONET retrievals yield values between approximately 1.46 and 1.58 depending on the days. Outside of the dust layer the retrieval of m_R is not reliable because the assumption of SVF=100% is not fulfilled and, as a result, the retrieved values of m_R are overestimated (Veselovskii et al., 2010).

The values of the imaginary part of the CRI retrieved from lidar measurements are approximately 0.007 inside the dust layer. However, the retrieved value is associated to average value over spectral range and characterized by high uncertainty (Müller et al., 2013). Still, this uncertainty does not affect significantly the retrieved values of volume and effective radius (Veselovskii et al., 2013.

The regularization approach estimates also the particle volume size distribution (PSD), allowing to conclude, which of the modes (fine or coarse) is predominant. Fig.18 shows the PSDs derived from lidar measurements on 10 April for four height layers of 150 m width centered at 1940, 3150, 4070, 4370 m heights. For the layers with strong dust loadings (1940, 3150 m) the coarse mode is dominant, at higher altitude outside the dust layer (4070, 4370 m), the fine mode (around 0.15µm) prevails. For comparison, the column integrated PSD obtained from AERONET level 1.5 data on 9 April at 18:00 UTC is also reported. The coarse mode looks shifted toward larger particles when compared to the lidar retrievals but the difference can be due to the spectral dependence of the imaginary part of m_I, as it will be discussed further in this section.

Depolarization measurements provide additional information about particle properties that can be used in the inversion algorithm as long as the forward model can compute the particle depolarization ratio with sufficient accuracy (Veselovskii et al., 2010; Müller et al., 2013). Hereinafter, we compare the retrieved aerosol parameters using 3β+2α or 3β+2α+1δ observations. To perform such a comparison we calculated the ratio of the effective radii (R_{δ}^{r}) derived from 3β+2α+1δ and 3β+2α sets. Fig.19 shows the profiles of R_{δ}^{r} for the same three days (right part associated with bottom x-axis); a value of 1.0 would mean that the additional input has no impact on the retrieval. Inside the dust layer the ratio is about 1.15 for the measurements taken on 13 and 29 of March. On 10 April, the ratio is noisier and more oscillating, but the average is still close to the results obtained for 13 and 29 March. Let us mention that the ratio of the particle volumes R_{δ}^{V} is very close to R_{δ}^{r}, so it is not shown in the figure. The increase of the effective radius (and volume) retrieved from 3β+2α+1δ measurements compared to 3β+2α occurs simultaneously with a decrease of the real and imaginary parts of CRI (Veselovskii et al., 2010; Müller et al., 2013). m_R and m_I decrease to values less than 1.45 and 0.005, respectively and are lower than expected based on in situ measurements (Müller et al., 2013). It may suggest that the spheroidal model has difficulty to reproduce high depolarization measurements. On March 13 and April 10, the depolarization ratio δ is decreasing above 2500m and 3700m (Figs 9 and 14 respectively) and we can notice that the value R_{δ}^{r} is then close to 1. Assuming that results obtained using 3β+2α data are more representative of the actual values, it means that the spheroidal model cannot reproduce high depolarization ratios reasonably well. Additional information brought by the depolarization ratio is so not suitable in such conditions.

The inversion results presented in fig.16, 17 are obtained assuming a spectrally independent refractive index while the imaginary part of CRI of dust is expected to increase in the UV spectral region. To test the effect of a spectrally dependent imaginary part $m_I(\lambda)$ on the retrieval, we now assume that the imaginary parts at 1064 nm and 532 nm wavelengths are the same $m_I(532) = m_I(1064)$, while $m_I(355) = 4m_I(532)$. Such an enhancement of m_I at 355 nm is quite typical for Saharan dust (Ansmann et al., 2011). The 3β+2α measurements for the same three days are so inverted assuming this $m_I(\lambda)$ spectral dependence as described in (Veselovskii et al., 2010). Fig.19 (left part associated with top x-axis) shows profiles of R_{mI}^{r}, which is the ratio of the effective radii retrieved under the assumption of spectrally dependent and spectrally independent imaginary part of RI. Again, the corresponding ratios R^{V}_{mI} for the volumes are close to R^{r}_{mI} and we do not report them. As expected, the effect of $m_I(\lambda)$ is more pronounced inside the dust layer, and on 29 March and 10 April (days characterized by negative BAE), the value of R^{r}_{mI} is up to 1.5. Accounting for $m_I(\lambda)$ dependence increases also the real part of RI, thus e on 29 March m_R increases from approximately 1.52 to 1.56 inside the dust layer. These model computations demonstrate that accounting for the spectral dependence of the imaginary part of RI in the dust layers may significantly increase the retrieved values of the effective radius and particle volume. In particular, it may explain smaller radii of the coarse mode particles retrieved from lidar measurements inside the dust layer (fig.19) when compared to AERONET results. The effects of spectral dependence of m_I can be to some extent corrected by using $m_I(\lambda)$ model based on in situ measurements and implying it in retrieval algorithm as described in (Veselovskii et al., 2010).

CONCLUSION

The lidar measurements performed in March-April 2015 during the first phase of the SHADOW campaign in Senegal has provided a significant amount of information about dust particle parameters. The use of rotational Raman scattering in the LILAS for 532 nm observations improved the α_{532} measurements and, as a result, the calculation of lidar ratio and extinction Ångström exponent were improved as well. The mean values of lidar ratios of pure dust were about 53±8 sr for both 532 nm and 355 nm wavelengths, which agrees with the values observed during SAMUM 1 (Morocco) and SAMUM 2 (Cape Verde) campaigns. The mean value of particle depolarization ratio at 532 nm was 30±4.5%, however during strong dust episodes this ratio increased up to 35±5%, which is also in agreement with the results of SAMUM campaigns. The backscattering Ångström exponent at 355/532 nm wavelengths during the dust episodes decreased to ~-0.7, while the EAE values, though being negative, were higher than -0.2. Low values of BAE may be a result of enhanced dust absorption at 355 nm.

The inversion of $3\beta+2\alpha$ measurements to particle microphysics in the case of dust is more challenging than other types of aerosols. The use of pure dust observations somewhat simplifies this task, because the contribution of the particles in the fine mode (which may have different origin) is insignificant. Moreover, in the retrieval of pure dust properties we don't need to consider the mixture of spheres and spheroids and can assume SVF=100%. The use of the spheroids model for the inversion of $3\beta+2\alpha$ measurements leads to values of effective radius in reasonable agreement with AERONET observations and yields reasonable values of the real part of RI. However, the use of depolarization measurements ($3\beta+2\alpha+1\delta$) in the inversion for pure dust, which is characterized by a depolarization ratio δ_{532} exceeding 30%, leads to values of effective radius and volume exceeding the corresponding values obtained from $3\beta+2\alpha$ measurements by a factor up to 1.15. At the same time, the values of m_R are decreased. These issues have already been discussed so at the current time we prefer to not use the depolarization ratio in the input data set for the inversion of dust particle parameters. We hope also that these discussions will stimulate development of the forward model accurately describing polarization properties of laser radiation backscattered by dust particles.

The analysis performed here demonstrates the importance of the spectral dependence of the imaginary part of RI in the UV spectral region. Model simulations demonstrate that including $m_I(\lambda)$ dependence may increase the values of effective radius and volume by a factor as large as 1.5. Thus, at the moment, dust particle microphysical properties obtained by inversion of lidar measurements may contain significant biases. Further research is needed to develop techniques correcting these biases in order the uncertainty of the estimates of r_{eff} and V to remain below 30%, which is a typical value when particles with prevailing fine mode are considered.

In addition to aerosol properties, the LILAS system provided profiles of the water vapor mixing ratio, which, being a conserved quantity, was frequently a convenient tracer that indicated the boundary between dry air masses transported over the continent and moist air masses transported over the ocean. The episodes considered in this paper were characterized mainly by low values of RH and the effects of the particles hygroscopic growth were not considered. Still, we have significant amount of the measurements in the condition of high RH, accompanied by formation of water and ice clouds near the dust layers. We plan to present these results in a separate publication.

During phase 1 of SHADOW the aerosols other than dust didn't occur in significant amount inside the height range available for the measurements, so this publication is focused mainly on the pure dust study. However in phase 2 the episodes of dust-smoke mixture were observed and such episodes provide opportunity to test the algorithm ability to profile the layers with different particle types. Such analysis is in progress and will be presented separately.

Acknowledgments: The authors are very grateful to IRD-Dakar (Institut de Recherche pour le Développement) for their welcome and efficient support and also thank the labex CaPPA for supporting this campaign. The CaPPA project (Chemical and Physical Properties of the Atmosphere) is funded by the French National Research Agency (ANR) through the PIA (Programme d'Investissement d'Avenir) under contract "ANR-11-LABX-0005-01" and by the Regional Council “ Nord-Pas de Calais » and the "European Funds for Regional Economic Development (FEDER)

References

Ansmann, A. and Müller, D.: Lidar and atmospheric aerosol particles, in “Lidar. Range-Resolved Optical Remote Sensing of the Atmosphere", Weitkamp, C. ed., Springer, New York, 2005, pp. 105-141.

Ansmann, A., Petzold, A., Kandler, K., Tegen, I., Wendisch, M., Müller, D., Weinzierl, B., Müller, T., Heintzenberg, J.: Saharan Mineral Dust Experiments SAMUM–1 and SAMUM–2: what have we learned?, Tellus, 63B, 403–429, 2011.

Ansmann, A., Seifert, P., Tesche, M., Wandinger, U.: Profiling of fine and coarse particle mass: case studies of Saharan dust and Eyjafjallajökull/Grimsvötn volcanic plumes. Atmos. Chem. Phys., 12, 9399–9415, 2012.

Balkanski, Y., Schulz, M., Claquin, T., and Guibert, S.: Reevaluation of mineral aerosol radiative forcings suggests a better agreement with satellite and AERONET data, Atmos. Chem. Phys., 7, 81–95, 2007.

Binietoglou, I., Basart, S., Alados-Arboledas, L., Amiridis, V., and co-authors: A methodology for investigating dust model performance using synergistic EARLINET/AERONET dust concentration retrievals. Atmos. Meas. Tech., 8, 3577–3600, 2015.

Browning, K. A. and Wexler, R.: The determination of kinematic properties of a wind field using Doppler radar, J., Appl. Meteor., 7, 105–113, 1968.

Burton, S. P., Vaughan, M. A., Ferrare, R. A. and Hostetler, C. A.: Separating mixtures of aerosol types in airborne High Spectral Resolution Lidar data. Atmos. Meas. Tech., 7, 419–436, 2014.

De Tomasi, F., Blanco, A., and Perrone, M. R..:Raman lidar monitoring of extinction and backscattering of African dust layers and dust characterization. Appl.Opt.42, 1699-1709, 2003.

Di Girolamo, P., Summa, D., Bhawar, R., Di Iorio, T., Cacciani, M., Veselovskii, I., Dubovik, O., Kolgotin, A.: Raman lidar observations of a Saharan dust outbreak event: characterization of the dust optical properties and determination of particle size and microphysical parameters, Atmospheric Environment. 50, 66-78, 2012.

Dubovik, O., Sinyuk, A., Lapyonok, T., Holben, B.N., Mishchenko, M., Yang, P., Eck, T.F., Volten, H., Munoz, O., Veihelmann, B., van der Zande, W.J., Leon, J.-F., Sorokin, M., Slutsker, I.: Application of spheroid models to account for aerosol particle nonsphericity in remote sensing of desert dust, *J. Geophys. Res*., 111, D11208, doi:10.1029/2005JD006619, 2006.

Esselborn, M., Wirth, M., Fix, A., Weinzierl, B., Rasp, K., Tesche, M., and Petzold, A.: Spatial distribution and optical properties of Saharan dust observed by airborne high spectral resolution lidar during SAMUM 2006, Tellus B, 61, 131–143, 2009.

Formenti, P., Schütz, L., Balkanski, Y., Desboeufs, K., Ebert, M., Kandler, K., Petzold, A., Scheuvens, D., Weinbruch, S., and Zhang, D.: Recent progress in understanding physical and chemical properties of African and Asian mineral dust, Atmos. Chem. Phys., 11, 8231-8256, doi:10.5194/acp-11-8231-2011, 2011.

Formenti P., A. Klaver, S. Chevaillier, E. Journet, J. Rajot, Mapping the physico-chemical properties of mineral dust in western Africa: mineralogical composition, Atmos. Chem.Phys., 14, 10663-1068, 2014.

Freudenthaler,V., Esselborn, M.,Wiegner, M.,Heese, B., Tesche, M. and co-authors: Depolarization ratio profiling at severalwavelengths in pure Saharan dust during SAMUM 2006, *Tellus* 61B, 165–179, 2009.

Gasteiger, J., Wiegner, M., Groß, S., Freudenthaler, V., Toledano, C., Tesche, M., and Kandler, K.: Modeling lidar-relevant optical properties of complex mineral dust aerosols, Tellus B, 63, 725-741, 2011.

Kandler, K., Lieke, K., Benker, N., Emmel, C., Küpper, M., Müller-Ebert,D., Ebert, M., Scheuvens, D., Schladitz, A., Schütz, L., Weinbruch, S.: Electron microscopy of particles collected at Praia, Cape Verde, during the Saharan Mineral Dust Experiment: Particle chemistry, shape, mixing state and complex refractive index. Tellus 63B, 475-496, 2011.

Klett J.D., “Lidar inversion with variable backscatter/extinction ratios”, Appl.Opt. 24, 1638-1643, 1985.

Kumer, V.-M., Reuder, J., Furevik, B.R.: A comparison of LiDAR and radiosonde wind measurements, Energy Procedia, 53, 214-220, 2014.

Li, W. J., and Shao, L. Y.: Observation of nitrate coatings on atmospheric mineral dust particles Atmos. Chem. Phys., 9, 1863–1871, 2009.

Mahowald, N. M., Kloster, S., Engelstaedter, S., Moore, J. K., Mukhopadhyay, S., McConnell, J. R., Albani, S., Doney, S. C., Bhattacharya, A., Curran, M. A. J., Flanner, M. G., Hoffman, F. M., Lawrence, D. M., Lindsay, K., Mayewski, P. A., Neff, J., Rothenberg, D., Thomas, E., Thornton, P. E., and Zender, C. S.: Observed 20th century desert dust variability: impact on climate and biogeochemistry, Atmos.Chem. Phys., 10, 10875-10893, 2010.

McConnell, C. L., Highwood, E. J., Coe, H., Formenti, P., Anderson, Osborne, B. S., Nava, S., Desboeufs, K., Chen, G., Harrison, M. A. J.: Seasonal variations of the physical and optical characteristics of Saharan dust: results from the Dust Outflow and Deposition to the Ocean (DODO) experiment, J. Geophys. Res. **113**, D14S05, doi:10.1029/2007JD009606, 2008.

Mishchenko, M.I., L.D. Travis, R.A. Kahn, and R.A. West, Modeling phase functions for dustlike tropospheric aerosols using a mixture of randomly oriented polydisperse spheroids, J. Geophys. Res., Vol. 102, 16831-16847, 1997

Mona, L., Amodeo, A., Pandolfi, M., Pappalardo, G.: Saharan dust intrusions in the Mediterranean area: three years of Raman lidar measurements. J. Geophys. Res., 111, D16203, doi:10.1029/2005JD006569, 2006.

Müller, D., Wandinger, U., and Ansmann, A.: Microphysical particle parameters from extinction and backscatter lidar data by inversion with regularization: theory, Appl. Opt. 38, 2346-2357, 1999.

Müller, D., Mattis, I., Wandinger, U., Ansmann, A., Althausen, D., Stohl, A.: Raman lidar observations of aged Siberian and Canadian forest fire smoke in the free troposphere over Germany in 2003: Microphysical particle characterization, J. Geophys. Res., 110, D17201, doi:10.1029/2004JD005756, 2005.

Müller, D., Weinzierl, B., Petzold, A., Kandler, K., Ansmann, A., Müller, T., Tesche, M., Freudenthaler, V., Esselborn, M., Heese, B., Althausen, D., Schladitz, A., Otto, S., and Knippertz, P.: Mineral dust observed with AERONET Sun photometer, Raman lidar and in situ instruments during SAMUM 2006: shape-independent particle properties, J. Geophys. Res., 115, D11207, doi:10.1029/2009JD012523, 2010.

Müller, D., Veselovskii, I., Kolgotin, A., Tesche, M., Ansmann, A., Dubovik, O.: Vertical profiles of pure dust (SAMUM-1) and mixed smoke-dust plumes (SAMUM-2) inferred from inversion of multiwavelength Raman/polarization lidar data and comparison to AERONET retrievals and in-situ observations, Appl.Opt. 52, 3178-3202, 2013.

Nisantzi, A., Mamouri, R. E., Ansmann, A., Schuster, G. L., Hadjimitsis, D. G.: Middle East versus Saharan dust extinction-to-backscatter ratios. Atmos. Chem. Phys., 15, 7071–7084, 2015.

Papayannis, A., Amiridis, V., Mona, L., Tsaknakis, G., Balis, D., Bösenberg, J., Chaikovski, A., De Tomasi, F., Grigorov, I., Mattis, I., Mitev, V., Müller, D., Nickovic, S., Pérez, C., Pietruczuk, A., Pisani, G., Ravetta, F., Rizi, V., Sicard, M., Trickl, T., Wiegner, M., Gerding, M., Mamouri, R. E., D'Amico, G., and Pappalardo, G.: Systematic lidar observations of Saharan dust over Europe in the frame of EARLINET (2000–2002), J. Geophys. Res., 113, D10204, doi:10.1029/2007JD009028, 2008.

Papayannis, A., Mamouri, R. E., Amiridis, V., Remoundaki, E., Tsaknakis, G., Kokkalis, P., Veselovskii, I., Kolgotin, A., Nenes, A., and Fountoukis, C.: Optical-microphysical properties of Saharan dust aerosols and composition relationship using a multi-wavelength Raman lidar, in situ sensors and modelling: a case study analysis, Atmos. Chem. Phys. 12, 4011-4032 (2012).

Patterson, E.M., Gillette, D.A., Stockton, B.H.: Complex Index of Refraction Between 300 and 700 nm for Saharan Aerosols, J. Geophys. Res. 82, 3153 - 3160, 1977.

Redelsperger, J.-L., Thorncroft, C. D., Diedhiou, A., Lebel, T., Parker, D. J., Polcher, J.: African Monsoon Multidisciplinary Analysis: an international research project and field campaign. Bull. Am.Meteorol. Soc. 87, 1739–1746, 2006.

Reid, J. S. and Maring, H. B: Foreword to special section on the Puerto Rico Dust Experiment (PRIDE), J. Geophys. Res. 108, 8585, doi:10.1029/2003JD003510, 2003.

Ruchith, R.D. and Ernest Raj, P.: Features of nocturnal low level jet (NLLJ) observed over a tropical Indian station using high resolution Doppler wind lidar, Journal of Atmospheric and Solar-Terrestrial Physics, 123, 113-123, 2015.

Sakai,T., Nagai,T., Nakazato,M., Mano,Y., and Matsumura, T: Ice clouds and Asian dust studied with lidar measurements of particle extinction-to-backscatter ratio, particle depolarization, and water-vapor mixing ratio over Tsukuba. Appl.Opt. 42, 7103-7116, 2003.

Schwanghart, W. and Schütt, B.: Meteorological causes of Harmattan dust in West Africa, Geomorphology, 95, 412-428, 2008.

Seibert, P., Beyrich, F., Gryning S., Joffre, S., Rasmussen, A., Tercier, P.: Review and intercomparison of operational methods for the determination of the mixing height, Atmospheric Environment, 34, 1001–1027, 2000.

Shimizu, A., Sugimoto, N., Matsui, I., Arao, K., Uno, I.,Murayama, T., Kagawa, N., Aoki, K., Uchiyama, A., Yamazaki, A.: Continuous observations of Asian dust and other aerosols by polarization lidars in China and Japan during ACE-Asia, J. Geophys. Res., 109, D19S17, doi:10.1029/2002JD003253, 2004.

Sokolik, I. N. and Toon, O. B.: Direct radiative forcing by anthropogenic airborne mineral aerosols, Nature, 381, 681–683, 1996.

Tanre, D., Haywood, J., Pelon, J., Leon, J.-F., Chatenet, B., Formenti, P., Francis, P., Goloub, P., Highwood, E. J., Myhre, G.: Measurements and modeling of the Saharan dust radiative impact: overview of the Saharan Dust Experiment (SHADE). J. Geophys. Res. 108, 8574, doi:10.1029/2002JD003273, 2003.

Tesche, M., Ansmann, A., Müller, D., Althausen, D., Engelmann, R., Freudenthaler, V., and Groß, S.: Vertically resolved separation of dust and smoke over Cape Verde using multiwavelength Raman and polarization lidars during Saharan Mineral Dust Experiment 2008, J. Geophys. Res., 114, D13202, doi:10.1029/2009JD011862, 2009a.

Tesche, M., Ansmann, A., Müller, D., Althausen, D., Mattis, I., Heese, B., Freudenthaler, V., Wiegner, M., Eseelborn, M., Pisani, G., and Knippertz, P.: Vertical profiling of Saharan dust with Raman lidars and airborne HSRL in southern Morocco during SAMUM, Tellus B, 61, 144–164, doi:10.1111/j.1600-0889.2008.00390.x, 2009b.

Tesche, M., Groß, S., Ansmann, A., Müller, D., Althausen, D., Freudenthaler, V., and Esselborn, M.: Profiling of Saharan dust and biomass-burning smoke with multiwavelength polarization Raman lidar at Cape Verde, Tellus B, 63, 649–676, doi:10.1111/j.1600-0889.2011.00548.x, 2011.

Thobois, L. and Soderholm, J.: Observing clear air close proximity environment of severe storms, Meteorological Technhology International, 9, 132-135, 2015.

Veselovskii I., Kolgotin, A., Griaznov, V., Müller, D., Wandinger, U., Whiteman, D.: Inversion with regularization for the retrieval of tropospheric aerosol parameters from multi-wavelength lidar sounding, Appl.Opt. 41, 3685-3699, 2002.

Veselovskii I., O. Dubovik, A. Kolgotin, T. Lapyonok, P. Di Girolamo, D. Summa, D. N. Whiteman, M. Mishchenko, and D. Tanré, 2010: Application Of Randomly Oriented Spheroids For Retrieval Of Dust Particle Parameters From Multiwavelength Lidar Measurements, J. Geophys. Res., **115**, D21203, doi:10.1029/2010JD014139, 2010.

Veselovskii I., D. N. Whiteman, M. Korenskiy, A. Kolgotin, O. Dubovik, D. Perez-Ramirez, A. Suvorina.: Retrieval of spatio-temporal distributions of particle parameters from multiwavelength lidar measurements using the linear estimation technique and comparison with AERONET, Atmos. Meas. Tech. 6, 2671-2682, 2013.

Veselovskii, I., Whiteman, D. N., Korenskiy, M., Suvorina, A., Kolgotin, A., Lyapustin, A., Wang, Y., Chin, M., Bian, H. Kucsera, T. L., Perez-Ramirez, D., Holben, B.: Characterization of forest fire smoke event near Washington, D.C. in Summer 2013 with multi-wavelength lidar. Atmos. Chem. Phys. 15, 1647–1660, 2015.

Veselovskii, I., Whiteman, D. N., Korenskiy, M., Suvorina, A., Perez-Ramirez, D.: Use of rotational Raman measurements in multiwavelength aerosol lidar for evaluation of particle backscattering and extinction, Atmos. Meas. Tech., 8, 4111–4122, 2015.

Wagner, J., Ansmann, A., Wandinger, U., Seifert, P., Schwarz, A., Tesche, M., Chaikovsky, A., Dubovik, O.: Evaluation of the Lidar/Radiometer Inversion Code (LIRIC) to determine microphysical properties of volcanic and desert dust, Atmos. Meas. Tech., 6, 1707–1724, 2013.

Whiteman, D., Melfi, S., Ferrare, R.: Raman lidar system for measurement of water vapor and aerosols in the Earth's atmosphere", Appl. Opt. 31, 3068-3082, 1992.

Wiegner, M., Gasteiger, J., Kandler, K., Weinzierl, B., Rasp, K., Esselborn, M., Freudenthaler, V., Heese, B., Toledano, C., Tesche, M., Althausen, D.: Numerical simulations of optical properties of Saharan dust aerosols with emphasis on lidar applications. Tellus 61B, 180–194, 2009.

Xie, C., Nishizawa,T., Sugimoto,N., Matsui,I., and Wang,Z.: Characteristics of aerosol optical properties in pollution and Asian dust episodes over Beijing, China. Appl.Opt. 47, 4945-4951, 2008.

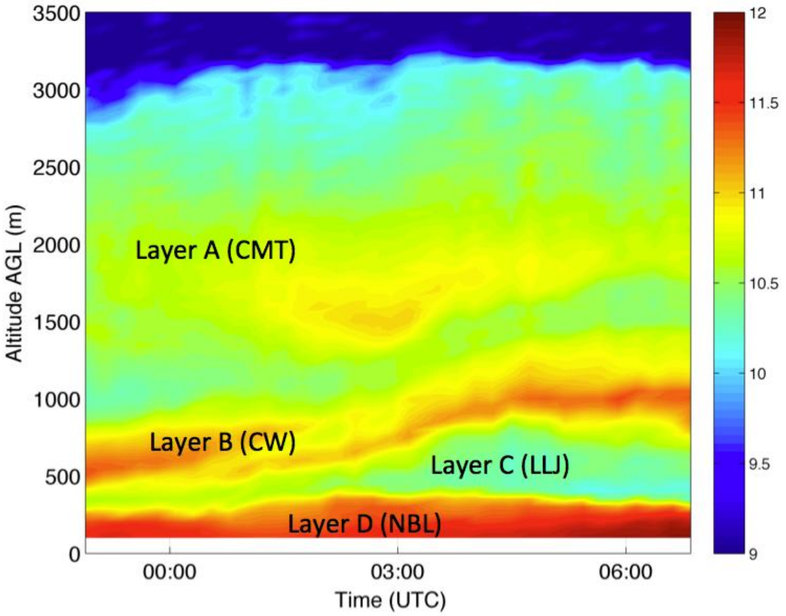

Fig.1. Time-height section of the logarithmic range corrected lidar signal (in arbitrary units) deduced from the Doppler lidar measurements during the 15-16 April 2015 night at Mbour. The stratification is represented by four layers: (A) continentalized maritime trade (CMT), (B) Layer advected mainly by a continental wind (CW), (C) low-level jet (LLJ) and (D) nocturnal boundary layer (NBL).

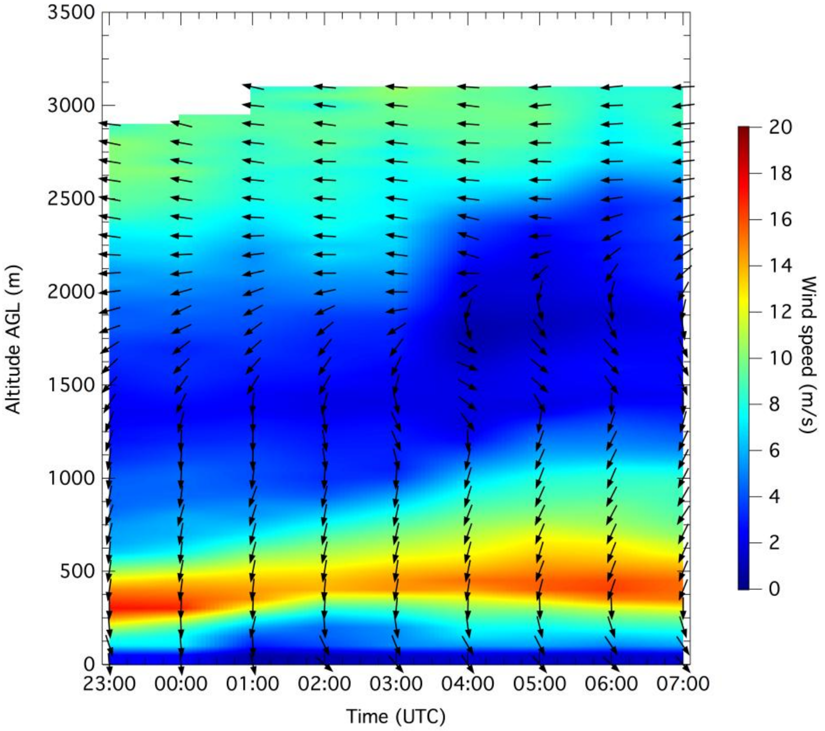

Fig. 2. Time-height section of horizontal wind direction (arrows) and wind speed (color map) deduced from Doppler lidar during 15-16 April. Leftward and downward arrows represent, respectively, easterly wind and northerly wind

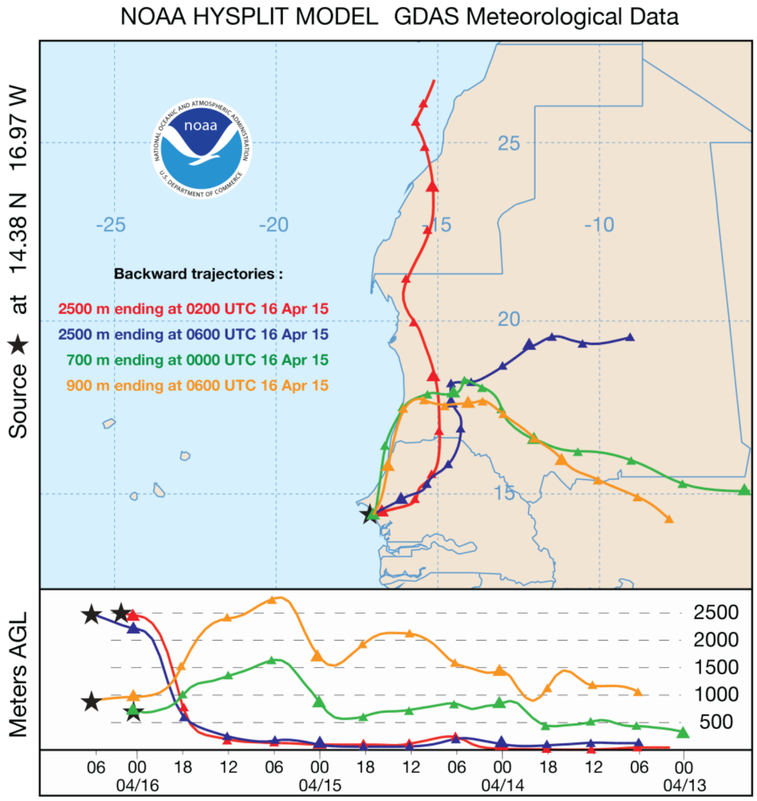

Fig.3. Back trajectories of the air masses ending in Mbour on 16 April 2015 at 2500 m (02:00 UTC, 06:00 UTC), at 700 m (00:00 UTC) and at 900 m (06:00 UTC). First two back trajectories correspond layer A from fig.1, while last two back trajectories correspond layer B from the same figure.

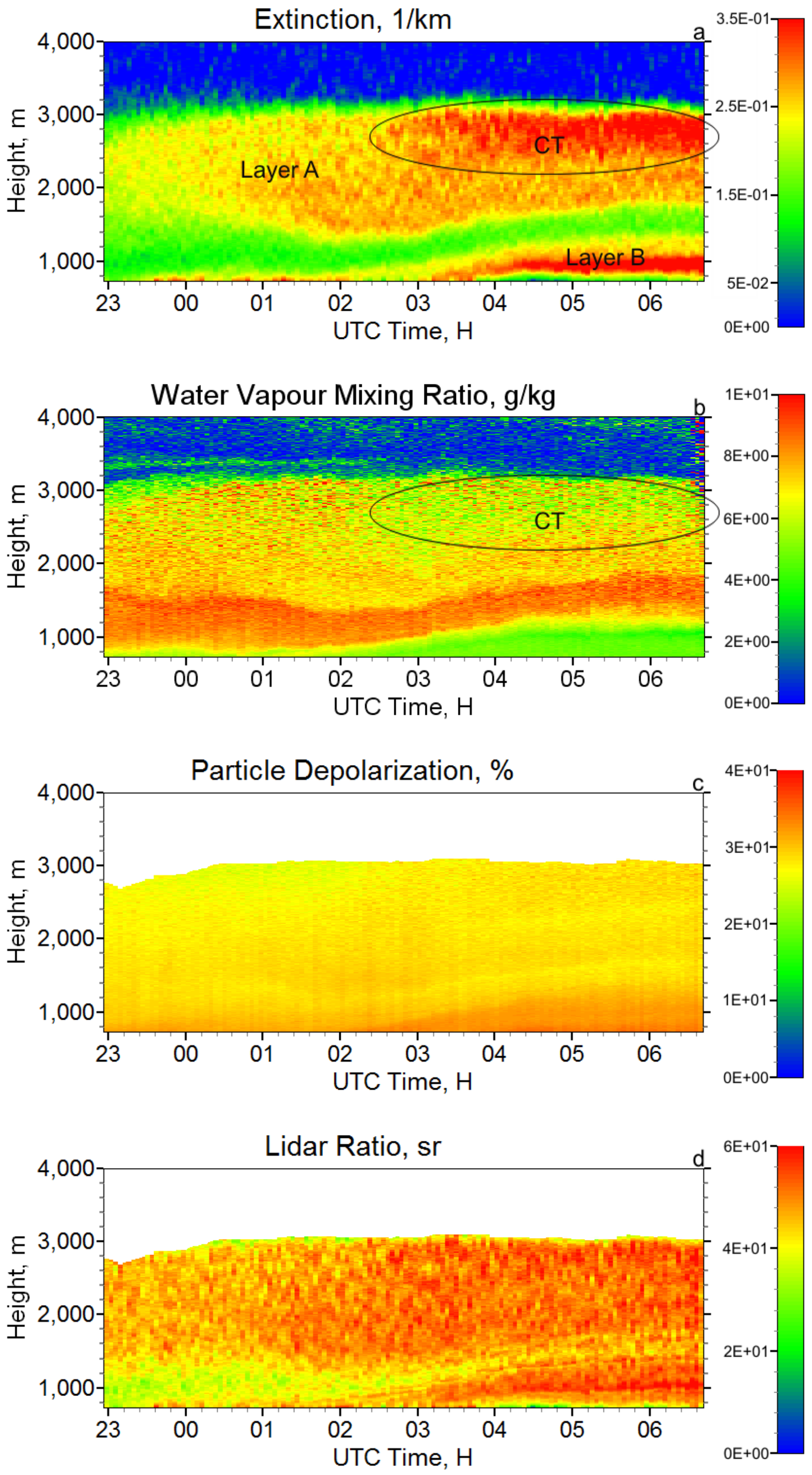

Fig.4. Height-temporal distribution of particle characteristics: (a) extinction α_{532}, (b) water vapor mixing ratio, (c) particle depolarization and (d) lidar ratio R_{532} measured during the 15-16 April night.

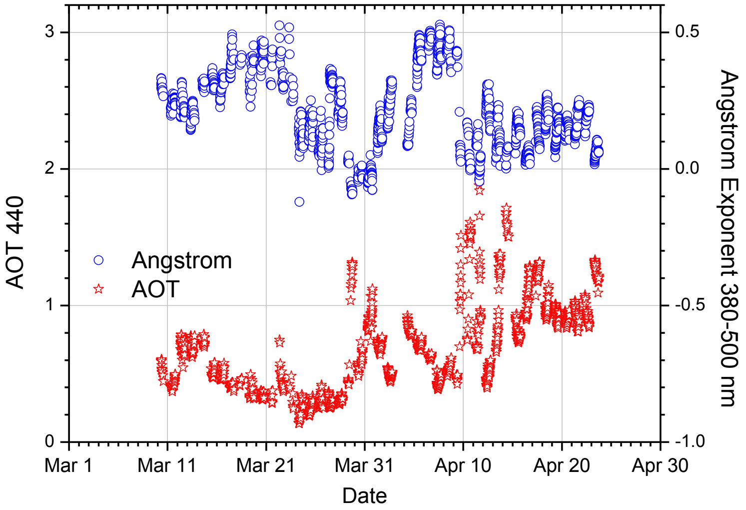

Fig.5. Aerosol optical thickness (AOT) at 440 nm and the extinction Ångström exponent at 380-550 nm wavelengths provided by AERONET in Mbour for March – April 2015 period.

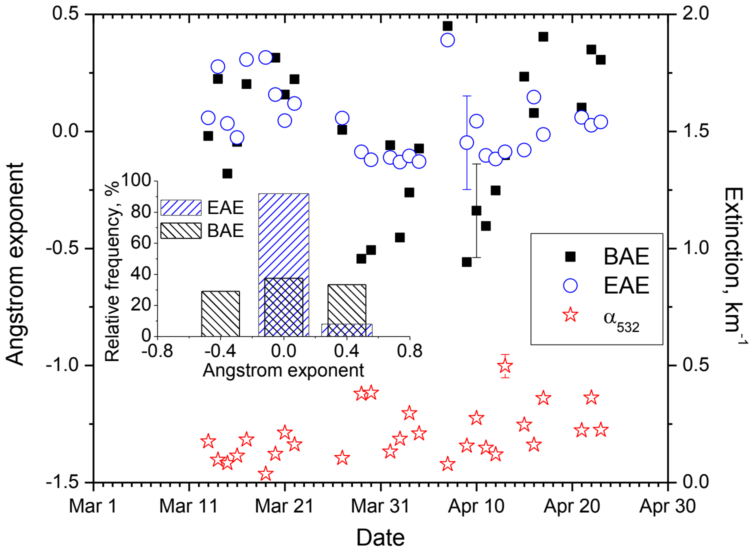

Fig. 6. Particle extinction at 532 nm together with backscattering and extinction Ångström exponents derived from lidar measurements within 1500 m – 2000 m layer for period March-April 2015. The insert shows the frequency distributions of BAE and EAE.

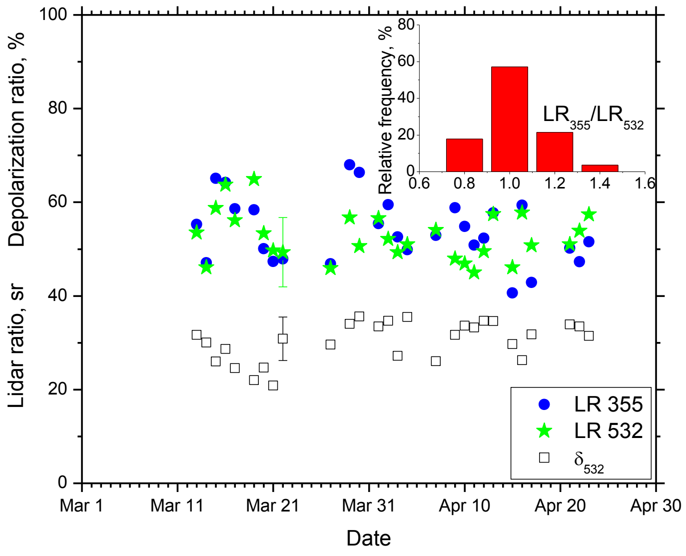

Fig. 7. Lidar ratios at 355 nm and 532 nm together with particle depolarization ratios derived from lidar measurements within 1500 m – 2000 m layer for period March-April 2015. The insert shows the frequency distribution of the ratio LR_{355}/LR_{532}.

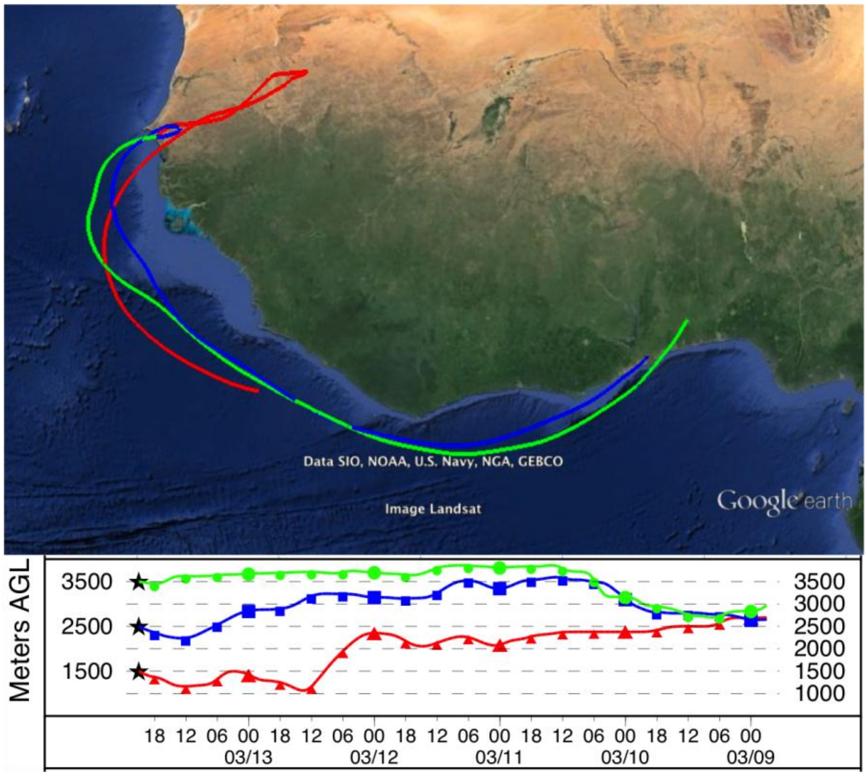

Fig.8. Five-day backward trajectories for the air mass in Mbour at altitudes 1500 m, 2500 m, 3500 m, on 13 March 2015 at 21:00 UTC.

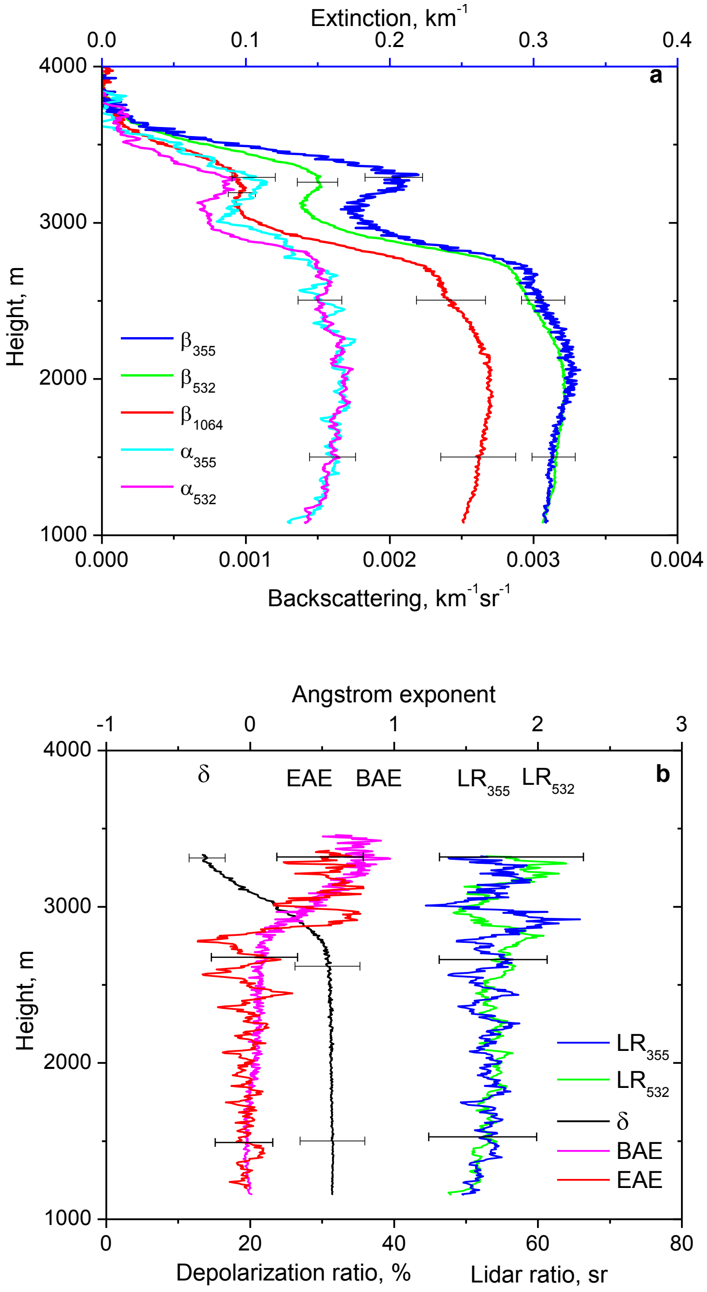

Fig.9. Vertical profiles of (a) backscattering and extinction coefficients and (b) lidar ratios, depolarization ratio, backscattering and extinction Ångström exponents at 355/532 nm measured on 13 March 2015 for period 20:30-21:30 UTC.

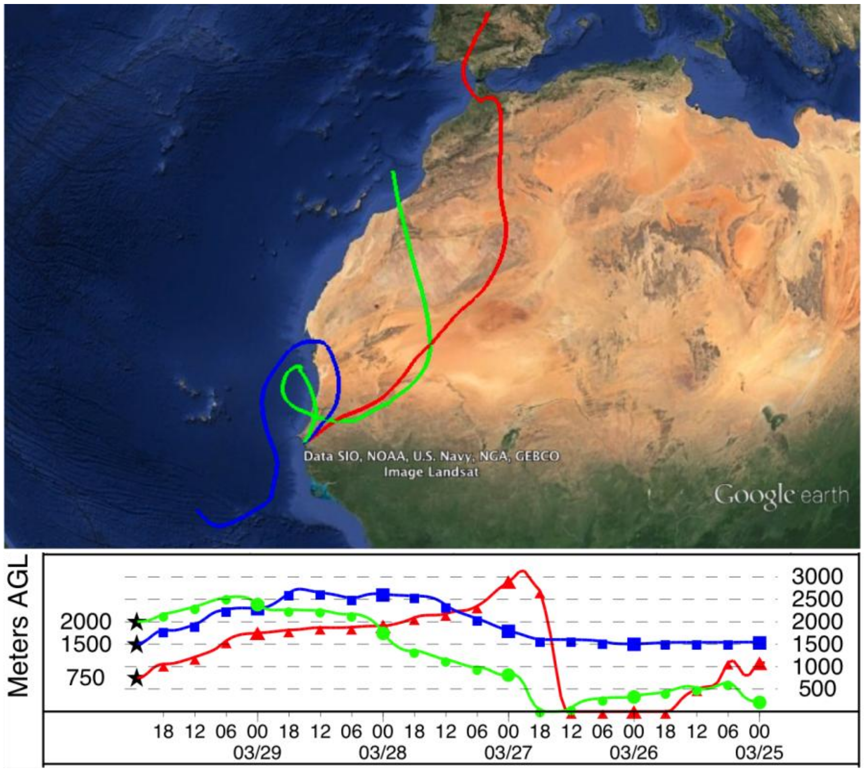

Fig.10. Five-day backward trajectories for the air mass in Mbour at altitudes 750 m, 1500 m, 2000 m on 29 March 2015 at 23:00 UTC.

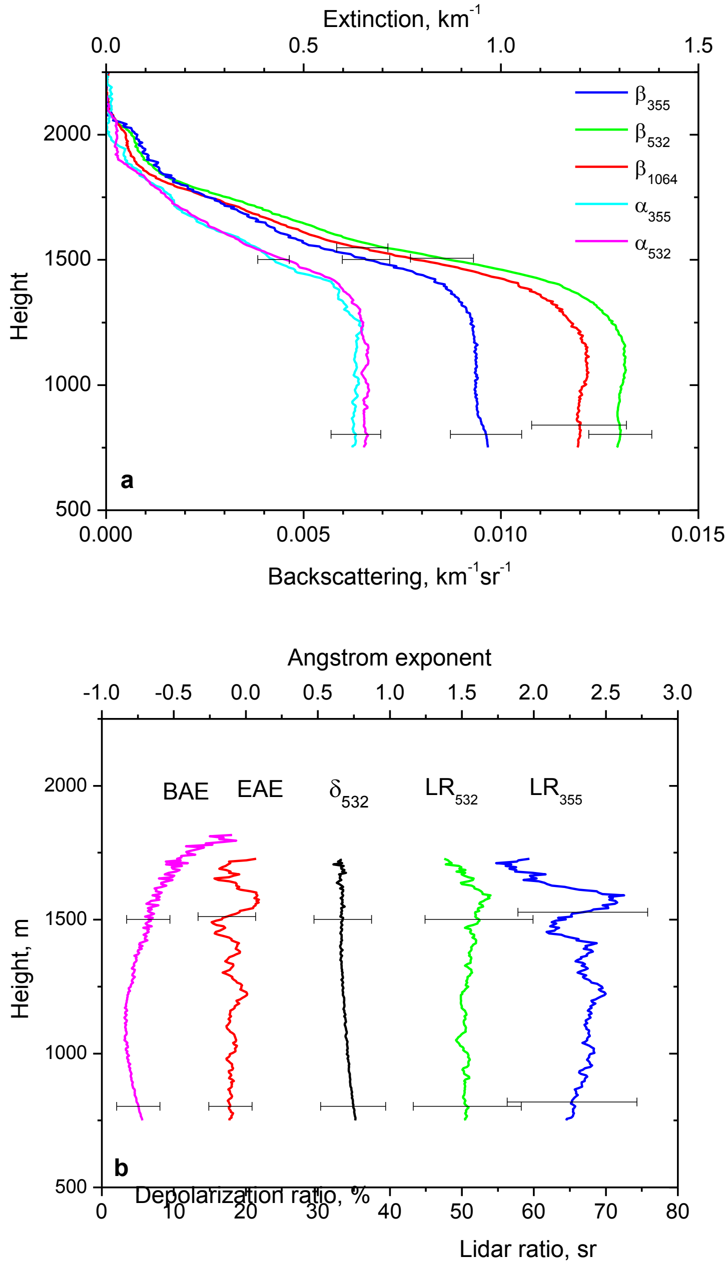

Fig.11. Vertical profiles of (a) backscattering and extinction coefficients and (b) lidar ratios, depolarization ratio, backscattering and extinction Ångström exponents measured on 29 March 2015 for period 22:00-23:30 UTC.

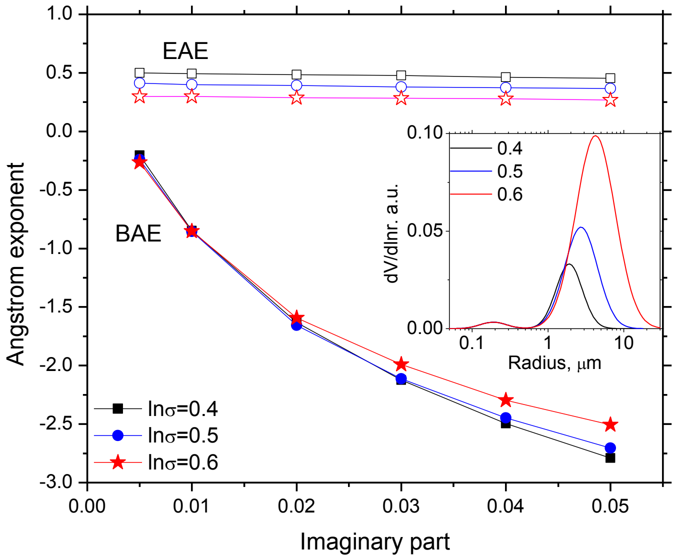

Fig.12. Extinction and backscattering Ångström exponent for 355/532nm wavelengths as a function of the imaginary part of the refractive index at 355 nm. The CRI at 532 nm was kept m=1.55-i.005. Computations were performed using the model of randomly oriented spheroids for three bimodal PSDs shown in the insert.

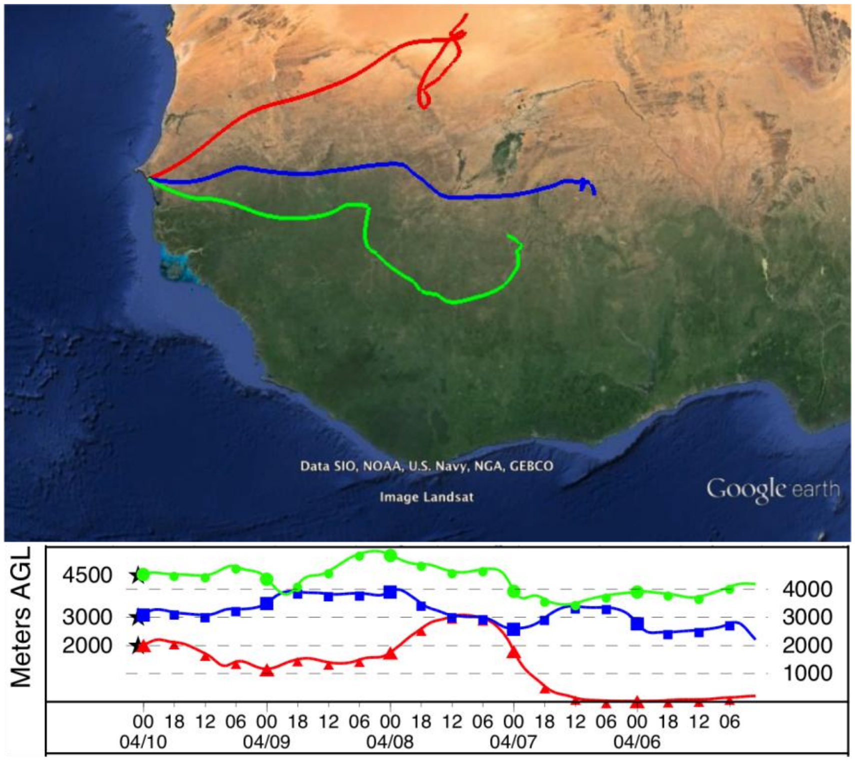

Fig.13. Five-day backward trajectories for the air mass in Mbour at altitudes 2000 m, 3000 m, 4500 m on 10 April 2015 at 01:00 UTC.

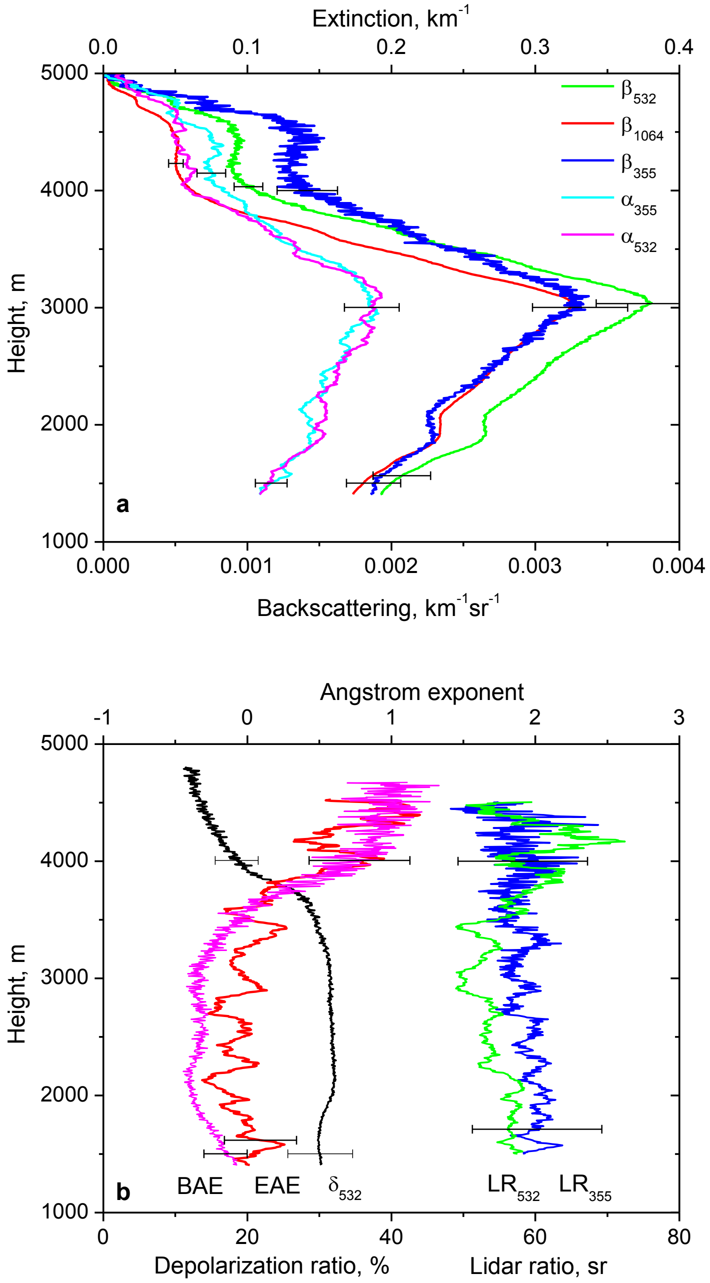

Fig.14 Vertical profiles of (a) backscattering and extinction coefficients and (b) depolarization ratio, backscattering and extinction Ångström exponents measured on 10 April 2015 for period 00:00-02:00 UTC.

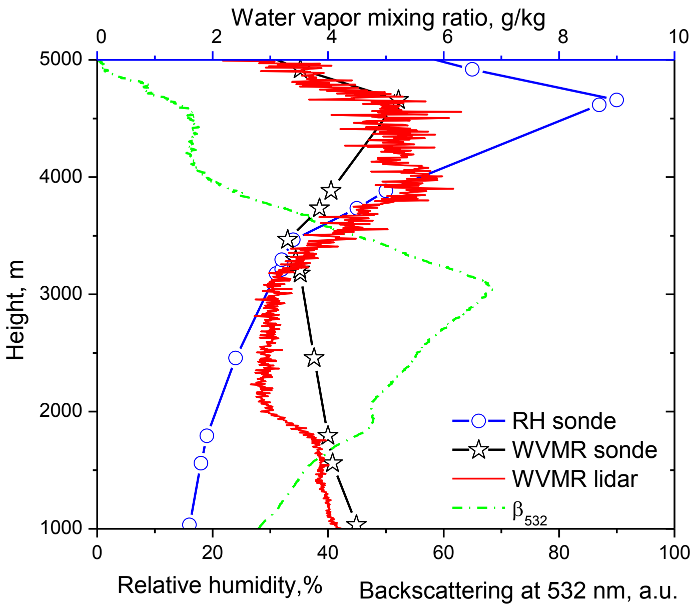

Fig.15. Vertical profile of water vapor mixing ratio (WVMR) measured with Raman lidar. The symbols show WVMR and the relative humidity (RH) measured with radio sonde in Dakar on 10 April at 00:00 UTC. Green dash-dot line shows backscattering coefficient at 532 nm.

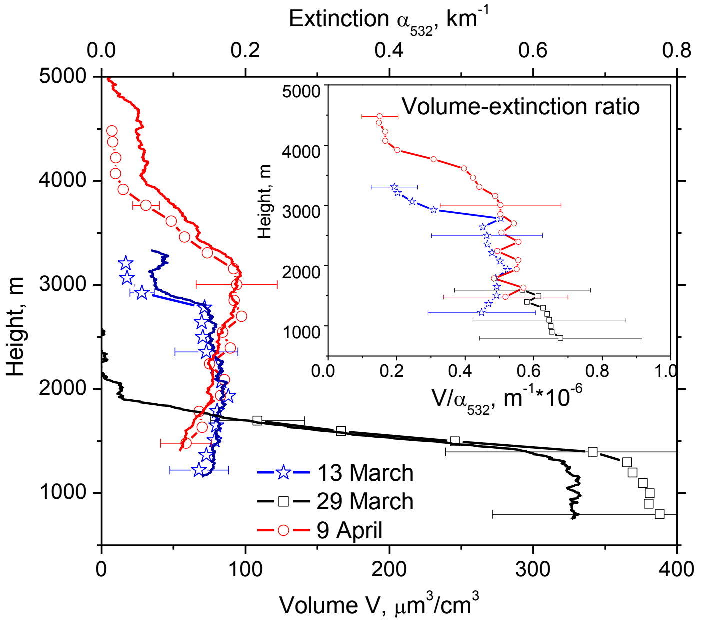

Fig.16. Vertical profiles of the particle volume density V retrieved from 3β+2α measurements on 13 March, 29 March and 10 April (symbols). Solid lines indicate the profiles of extinction coefficient at 532 nm. The insert shows the volume – extinction ratio V/α_{532} for the days considered.

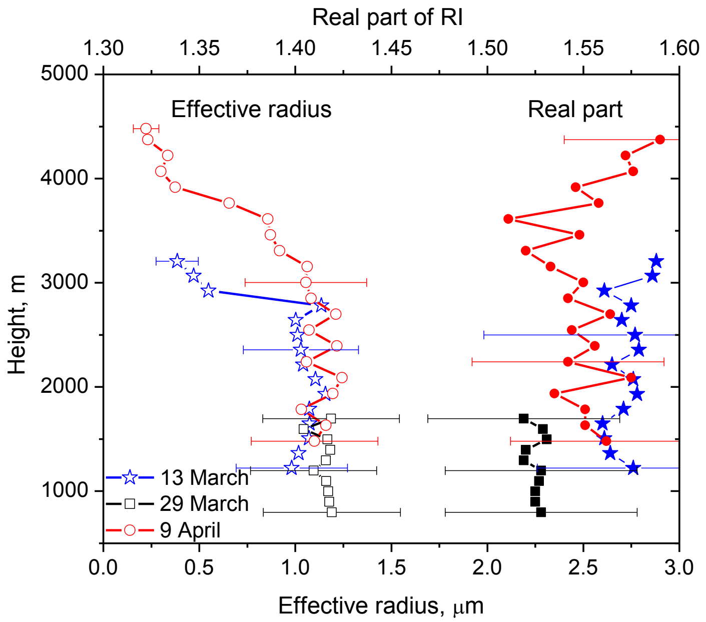

Fig.17. The profiles of (open symbols) the particle effective radius and (solid symbols) the real part of RI retrieved from 3β+2α measurements on 13 March, 29 March and 10 April.

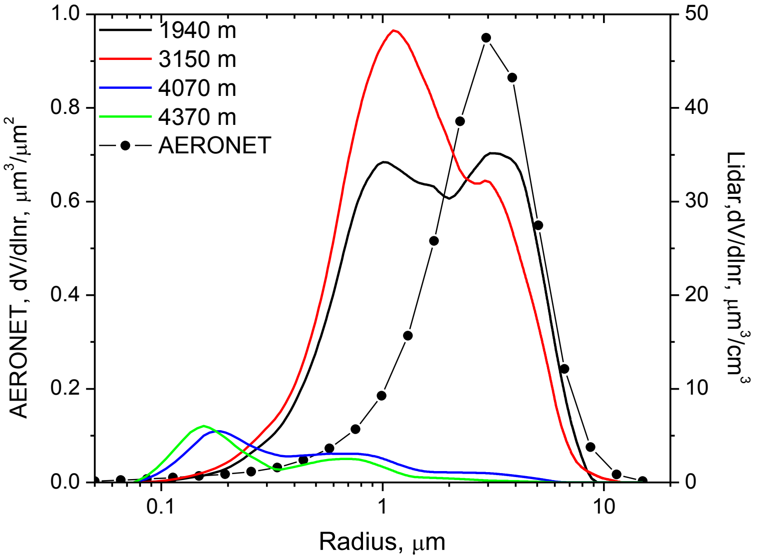

Fig.18. Particle size distributions retrieved from the measurements on 10 April for four height layers 1940, 3150, 4070, 4370 m. Symbols show the PSD provided by AERONET on 9 April at 18:00 UTC, inversion level 1.5.

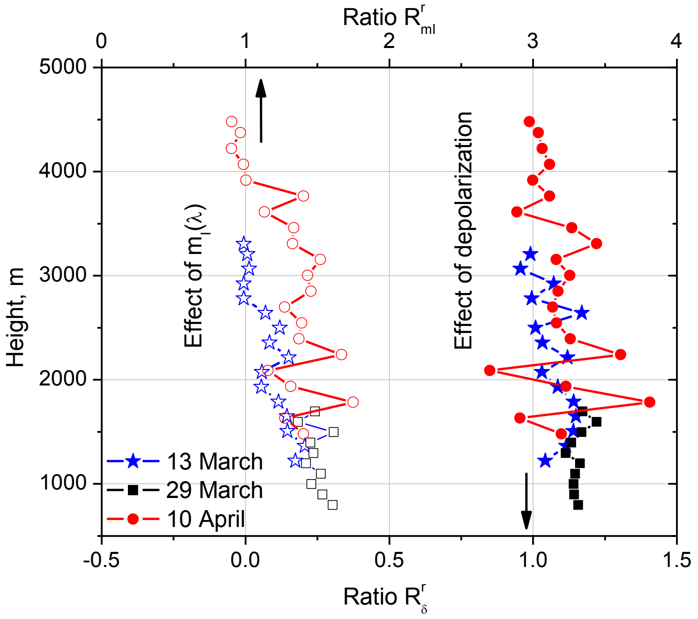

Fig. 19. Enhancement of retrieved effective radius due to using the particle depolarization ratio in input data set (R_δ^r) and due to accounting for the spectral dependence of the imaginary part of RI (R_{mI}^r).Shown are results for the measurements on 13 March, 29 March and 10 April 2015.